

A fast test for the identification and confirmation of massive black hole binary

Massimo Dotti^{1,2,3,*}, Fabio Rigamonti^{4,2,3}, Stefano Rinaldi^{5,6}, Walter Del Pozzo^{5,6}, Roberto Decarli⁷, and Riccardo Buscicchio^{1,2}

¹ Università degli Studi di Milano-Bicocca, Piazza della Scienza 3, 20126 Milano, Italy

² INFN, Sezione di Milano-Bicocca, Piazza della Scienza 3, I-20126 Milano, Italy

³ INAF - Osservatorio Astronomico di Brera, via Brera 20, I-20121 Milano, Italy

⁴ DiSAT, Università degli Studi dell'Insubria, via Valleggio 11, I-22100 Como, Italy

⁵ Dipartimento di Fisica "E. Fermi", Università di Pisa, I-56127 Pisa, Italy

⁶ Istituto Nazionale di Fisica Nucleare, Sezione di Pisa, I-56127 Pisa, Italy

⁷ INAF – Osservatorio di Astrofisica e Scienza dello Spazio di Bologna, Via Gobetti 93/3, I-40129 Bologna, Italy

Received XXX; accepted YYY

ABSTRACT

We present a new observational test to identify massive black hole binaries in large multi-epoch spectroscopical catalogues and to probe the real nature of already proposed binary candidates. The test is tailored for binaries with separations large enough to allow each black hole to retain its own broad line region. In this limit the fast AGN variability typically observed over months cannot be associated to the much longer binary period, and it is assumed (as for the case of single black holes) to be the consequence of the evolution of the innermost regions of the two accretion discs. A simple analysis of the cross-correlation between different parts of individual broad emission lines can therefore identify the presence of two massive black holes whose continua vary independently of each other. Our analysis indicates that to be less affected by the noise in the spectra the broad lines should be divided in two close-to-equal-flux parts. This ensures that in the single massive black hole scenario the cross-correlation will always be high. With monitoring campaigns similar to those performed for reverberation mapping studies, on the other way, a binary can show any value of the cross-correlation and can therefore be distinguished from a standard AGN. The new test can be performed over timescales orders of magnitude shorter than the alternative tests already discussed in literature, and can be a powerful complement to the massive black hole binary search strategies already in place.

Key words. accretion – accretion discs – galaxies: interactions – quasars: supermassive black holes – quasars: emission lines – techniques: spectroscopic

1. Introduction

Gravitationally bound massive black hole (MBH) binaries (MBHBs), outcome of galaxy mergers predicted since Begelman et al. (1980), are among the loudest sources of gravitational waves (GWs) detectable with current pulsar timing array (PTA) campaigns (Verbiest et al. 2016) and by future space-based gravitational wave interferometers (e.g. LISA Amaro-Seoane et al. 2017, 2023). The GW background generated by MBHBs as well as the rate of detectable binary coalescences are still quite uncertain, in part as a consequence of the uncertainties on the efficiency of MBH pairing during the early stages of galaxy mergers (Fiacconi et al. 2013; del Valle et al. 2015; Tamburello et al. 2017; Souza Lima et al. 2017; Bortolas et al. 2020, 2022). The electromagnetic (EM) identification of a sample of already bound MBH binaries would therefore greatly reduce the uncertainties on the signals observable with both PTA and LISA.

To date, unfortunately, a definite observational confirmation of any MBHB has not been found yet. The only spatially resolved MBHB candidate is 0402+379 (Rodríguez et al. 2009; Burke-Spolaor 2011), having two flat-spectrum radio cores with a projected separation of ≈ 7 pc.

At smaller, spatially unresolved, scales, MBHBs have been consistently searched for either through peculiar spectral features (Tsalmantza et al. 2011; Eracleous et al. 2012; Ju et al. 2013; Shen et al. 2013; Wang et al. 2017) or through photometric variability (Valtonen et al. 2008; Ackermann et al. 2015; Graham et al. 2015; Li et al. 2016; Charisi et al. 2016; Sandrinelli et al. 2016, 2018; Severgnini et al. 2018; Li et al. 2019; Liu et al. 2019; Chen et al. 2020).

These two search strategies target MBHBs at different separations. The spectroscopic approach assumes that the broad line region (BLR) of at least one of the binary components does not extend out of its MBH Roche radius. The broad emission lines (BELs), therefore, by sharing the same kinematics of the MBH, are shifted in frequency with respect to the host galaxy rest frame and evolve in time over a binary orbital period τ_{orb} . The constraint on the size of the BLR can be translated in a constraint on the minimum binary separation, of the order of ~ 0.1 pc for a $10^8 M_{\odot}$ MBH accreting at a tenth of its Eddington ratio (see section 2 for more details).

At smaller separations the BLR is either truncated by the time-dependent binary potential (Montuori et al. 2011) or shared by both MBHs and comoving with the MBHB centre of mass. Theoretical studies predict periodic variability on timescales of $\sim \tau_{\text{orb}}$, either associated to the periodic fueling from the circum-

* massimo.dotti@unimib.it

binary material (e.g. Hayasaki et al. 2008) or to the Doppler boosting of the emission for very close binaries (D’Orazio et al. 2015). At close separations such timescales can get as short as $\lesssim 1$ yr, allowing for observational searches in current and future multi-epoch observations (see Graham et al. 2015; Charisi et al. 2016; Liu et al. 2019; Chen et al. 2020, and references therein).

Unfortunately, all the above-mentioned features used to identify MBHB candidates can have alternative explanations (see Dotti et al. 2023, for an overview of the possible alternative interpretations). The theoretical prediction of clear, unique, and observational features associated with MBHBs is therefore needed in order to test the actual binary nature of both small (selected through their variability) and large (spectroscopically identified) scales MBHB candidates. Some tests have recently been proposed for the small scales MBHB candidates, including the possibility of periodic gravitational lensing from the companion of the active component of the MBHB (for binaries observed nearly edge-on, see e.g. D’Orazio & Di Stefano 2018; Davelaar & Haiman 2022b,a) and periodic evolution of the polarization fraction and angle (Dotti et al. 2022).

For larger separation MBHBs, (e.g. Gaskell 1996; Eracleous et al. 1997) a straightforward test consists in observing the expected Doppler drift in the BEL profiles according to the motion of the active component (or components, if both MBHBs are active) of the binary with a τ_{orb} period (e.g. Gaskell 1996; Eracleous et al. 1997). A conclusive test would require to follow the system spectroscopically for $\sim \tau_{\text{orb}}$. At these scales, however, τ_{orb} can be as high as $\gtrsim 10 - 100$ yr (see section 2) making such test (dubbed slow periodicity test - SPT - hereon) challenging and unpractical for some of the candidates (see, e.g. Eracleous et al. 2012; Decarli et al. 2013; Runnoe et al. 2017).

In this paper, we propose a new test for the same large separation binary candidates, based on the assumption that at such large separations the short ($\lesssim 1$ day) timescale intrinsic accretion variability is unrelated to the binary period, and that, when both MBHBs are active, their variability patterns are uncorrelated. Such variability reverberates on the MBH BLRs (e.g. Blandford & McKee 1982). As we will argue in the following, dividing the BELs in two components (a “red” and a “blue” one, that together account for the total flux in the BEL) and cross-correlating the time-evolution of their fluxes can allow for the identification of MBHBs. Indeed, in the binary scenario, each observed BEL would be composed by two different broad lines, each with a different velocity offset with respect to the galaxy rest frame, and with the two components varying independently. In this scenario the cross-correlation between the blue and red parts of the BELs can be significantly smaller with respect to the case of an AGN powered by a single MBH, as long as the velocity offset is not negligible (i.e. each component associated to one of the MBHBs contributes significantly to one of the blue or red parts of the global BEL). This implies that our test becomes less and less effective for larger and larger binary separations, with a cross-correlation between the two different parts of the BEL getting closer and closer to the high values expected for single MBHBs, and failing to detect any true binary for close to zero relative line-of-sight velocity between the two MBH (see section 4). However, while other proposed spectroscopical tests are expected to fail when the velocity shift between the two components equal to their width (e.g. Shen & Loeb 2010), in section 4 we will demonstrate that our test can still identify binaries at larger separations/smaller velocity shifts, including binaries with periods up to ~ 1000 yr.

Our proposed method can be thought as a simplified version of the tests proposed by Wang et al. (2018); Songsheng et al.

(2020), in which a catalogue of two dimensional transfer function (TF) for a different binaries is constructed and compared to the full TF of the candidate in exam. While our method is clearly less sensible to the details of the BEL profile variability, it allows for a fast and quantitative check of the “binary” nature of the candidate even when the quality of the data can hardly constrain the details of the TF.

The clearest advantage of our new test (dubbed fast uncorrelated variability test - FUVT) is that it can be performed over timescales comparable to the typical duration of the reverberation mapping (RM) campaigns (e.g. Bentz et al. 2009b), usually smaller than a yr (down to weeks, orders of magnitude smaller than τ_{orb}). A second advantage is that, while FUVT can be applied to already identified MBHB candidates with shifted, asymmetric or double-peaked broad emission lines, it can also be used to identify new binaries with apparently “standard” BELs in large multi-epoch samples of AGNs.

This paper is organised as follows: in § 2 we describe the timescales required by FUVT and its range of applicability in terms of intrinsic MBHB properties; in § 3 we describe how the FUVT is structured, and we present the results of its application to a real sample of type I AGN (sample I hereon) studied through reverberation mapping; § 4 explains how a mock catalogue of MBHBs (sample II) has been constructed starting from sample I, and the results of the application of FUVT to the new binary sample; we then conclude with § 5 by summarizing the main results of our study, describing the advantages and disadvantages of FUVT with respect to SPT, and discussing how future observations can further strengthen the test payoff.

2. Analytical estimates of FUVT range of applicability

As commented in the introduction, both SPT and FUVT assume that both the BLRs are bound to and comoving with the individual components of the binary.

The BLR radius depends on the BEL we are focusing on and on the luminosities of the accreting MBHBs. For the broad H β line (that will be used in the following) the BLR radius is (Bentz et al. 2009a):

$$R_{\text{B-H}\beta} \approx 34 \text{ light day} \times \left(\frac{\lambda L_{\lambda,5100}}{10^{44} \text{ erg s}^{-1}} \right)^{0.519}, \quad (1)$$

where $\lambda L_{\lambda,5100}$ is the monochromatic luminosity of the AGN continuum at 5100 Å. Assuming that the bolometric luminosity is $L_{\text{bol}} \approx 9 \lambda L_{\lambda,5100}$ (Kaspi et al. 2000) we can express eq. 1 as a function of the individual MBH mass M and its Eddington ratio $f_{\text{Edd}} = L_{\text{bol}}/L_{\text{Edd}}$:

$$R_{\text{B-H}\beta} \approx 11 \text{ light day} \times \left(f_{\text{Edd}} \frac{M}{10^6 M_{\odot}} \right)^{0.519}. \quad (2)$$

This radius is required to be smaller than the Roche lobe radius of each individual MBH (Montuori et al. 2011). For the test to work the fluxes from the two accretion discs (hence the BLR radii) have to be comparable. Therefore the minimum separation between the two MBHBs is set by the Roche lobe of the secondary MBH, that for circular binaries is (Eggleton 1983):

$$R_{\text{RL},2} \approx 0.49 a \frac{q^{2/3}}{0.6 q^{2/3} + \ln(1 + q^{1/3})}, \quad (3)$$

where a is the separation between the two MBHBs and $q = M_2/M_1$ is the ratio between the secondary and the primary masses.

The minimum separation of the binary and, assuming circular Keplerian orbits, the minimum value of τ_{orb} for which both SPT and FUVT are applicable is obtained by equating eq. 2 and eq. 3:

$$\tau_{\text{orb,min}} \approx 200 \text{ yr } f_{\text{Edd},2}^{0.78} \left(\frac{M_2}{10^6 M_\odot} \right)^{0.28} \sqrt{\frac{[0.6 q^{2/3} + \ln(1 + q^{1/3})]^3}{q(1+q)}}, \quad (4)$$

where $f_{\text{Edd},2}$ is the Eddington ratio of the secondary. It is interesting to note that $\tau_{\text{orb,min}}$ has a stronger dependence on $f_{\text{Edd},2}$ than that on the M_2 . At fixed luminosity, therefore, shorter minimum periods are expected for higher MBH masses. Secondary MBHs of $10^8 M_\odot$, as for the spectroscopic MBHB candidates proposed to date (e.g. Tsalmantza et al. 2011; Eracleous et al. 2012), could be in binaries with minimum periods as small as ~ 27 yr (see also Decarli et al. 2013; Runnoe et al. 2017), if accreting at $f_{\text{Edd},2} = 0.01$, i.e. with the same bolometric luminosity as a $10^6 M_\odot$ accreting at its Eddington limit.

Note however that for disc-like BLRs the region within which circular orbits around a single MBH are stable is sizeably smaller (by a factor of $\approx 4 - 5$) than the Roche lobe (e.g. Eggleton 1983; Runnoe et al. 2015). On top of this consideration, gas at distances $> R_{\text{B-H}\beta}$ contribute to the central part of the broad H β line, and, if the binary separation is too small, such a contribution would be lost and the line would acquire a “boxy” profile¹. In the following we will consider both binaries with periods corresponding to BLR sizes similar to the secondary Roche lobe, and binaries with significantly larger periods, for which a stable disc-like BLR can survive around each of the two MBHs (see section 4).

Finally, the typical timescale for the H β reverberation to the change of the continuum can be estimated as $\tau_{\text{B-H}\beta} = R_{\text{B-H}\beta}/c$ (where c is the speed of light). Such time-scale has been evaluated through reverberation mapping and ranges from days to months depending on the luminosity of the accreting MBH. Reverberation mapping studies, however, typically require longer durations, even for $\sim 10^6 M_\odot$ MBHs, due to the need of sufficiently long baselines and sufficiently varying continua to allow for the test. As a consequence, the typical timescales needed to probe the variability both in the continuum and in the BELs are of the order of weeks to months (Bentz et al. 2009b).

3. FUVT description and results on a control sample of single MBHs

We apply FUVT to nine AGN for which $\tau_{\text{B-H}\beta}$ (and, therefore, masses) have been obtained in Bentz et al. (2009b): Mrk 142, SBS 1116+583A, Arp 151, Mrk 1310, Mrk202, NGC 4253, NGC 4748, NGC 5548, NGC 6814. We will assume as a working hypothesis that the whole sample is composed by only bona-fide single MBHs, and use it as a comparison for the mock binary sample described in the next section. We stress, however, that at least one of the AGN in sample I (NGC 5548) has been proposed as a binary candidate (Li et al. 2016) based on the variability of the periodic modulation of its broad H β line.

For all AGN Bentz et al. (2009b) have estimated delays between the continuum and the broad H β in between 2 and 7 days

and masses in the $1 - 7 \times 10^6 M_\odot$ range, with the exception of NGC 6814, with mass $\approx 1.85 \times 10^7 M_\odot$, and NGC 5548, with mass $8.2 \times 10^7 M_\odot$ (see Bentz et al. 2009b, for additional details on the properties of the single AGNs).

For our analysis we used scaled spectra, released by the Authors after the application of a re-normalization used to set the flux of all spectra to a consistent scale. For every AGN we removed the mean spectrum (averaged over all the observations) and worked on the variable part of the spectra only, dominated by the AGN continua and the BELs. We then removed the AGN continuum by fitting a straight line to the spectrum near the H β BEL, using the same wavelength intervals used in Bentz et al. (2009b).²

For each AGN we then compute the root-mean-square (RMS) spectrum. We use it to identify seven $\bar{\lambda}$ dividing the RMS broad H β in eight equal-flux parts³. For each $\bar{\lambda}$ in each spectrum we divide the H β BEL in two components, a red one and a blue one (r-H β and b-H β , for wavelengths longer and shorter than $\bar{\lambda}$, respectively). We then compute the light curves of the r-H β and b-H β components, and perform the cross-correlation between the two, allowing for a small time-shift τ_{shift} in the $[-10 \text{ day}, 10 \text{ day}]$ interval to take into account different reverberation times for different parts of the broad lines (due to e.g. the inflowing or outflowing BLR dynamics, e.g. Bentz et al. 2009b). More specifically we follow the standard RM practice of first using one lightcurve and interpolate the other, then to swap the two and repeat the exercise. The average cross-correlation is then used, and the uncertainties on the the cross-correlation and τ_{shift} are estimated using the PYTHON public version (Sun et al. 2018)⁴ of the Monte Carlo code discussed in Peterson et al. (1998, 2004).

For each AGN and each $\bar{\lambda}$ we measure $\max - \text{CCF}(\bar{\lambda})$, i.e. the maximum value of the r-H β -b-H β cross-correlation, and its uncertainties. The $\max - \text{CCF}(\bar{\lambda})$ obtained following this procedure are shown in figure 1 for NGC 4748. The peak of $\max - \text{CCF}(\bar{\lambda})$ ($\overline{\text{CCF}}$ hereafter)⁵ corresponds to the $\bar{\lambda}$ threshold dividing the broad H β line in two equal-flux parts, while the cross-correlation decreases significantly (and its uncertainties increase) when moving $\bar{\lambda}$ toward the line wings, more affected by the noise in the spectra. More in general in the sample the values of $\overline{\text{CCF}}$ are comparable or slightly higher than the peak of the cross-correlations between the whole broad H β and the photometric B and V light-curves shown in Bentz et al. (2009b). The trends discussed for NGC 4748 are common for all the nine AGN we examined: $\overline{\text{CCF}}$ is always found in the bulk of the line (hereby defined as the region in between the third and the fifth values of $\bar{\lambda}$, i.e. when the less luminous part of the BEL has at least 3/8 of the total BEL flux), and it is always $\gtrsim 0.75$.⁶

² Although our procedure is slightly different from the one used in Bentz et al. (2009b), we recover the same fluxes (within uncertainties) of the whole broad H β for every pointing of every AGN.

³ The number of $\bar{\lambda}$ is indeed somewhat arbitrary. We used eight as it is the maximum number of bins used in Bentz et al. (2009b) for 2D reverberation mapping of the nine single MBH, in order to keep a sufficiently high signal-to-noise ratio in each frequency bin.

⁴ We modified the public version to output the uncertainties on the cross-correlation, too.

⁵ We stress again that $\overline{\text{CCF}}$ refers to the maximum CCF over all the possible $\bar{\lambda}$ while $\max - \text{CCF}(\bar{\lambda})$ refers to the maximum CCF for a specific $\bar{\lambda}$.

⁶ The profiles of $\max - \text{CCF}(\bar{\lambda})$ for all the other single MBHs as well as for all the mock binaries discussed in the next section are available at <https://astro.fisica.unimib.it/spectroscopical-search-of-massive-black-hole-binaries/>

¹ A boxy profile is not an unequivocal signature of a binary. Indeed, some of the observed AGN discussed in section 3 have boxy profiles, see e.g. the mean spectra in Bentz et al. (2009b).

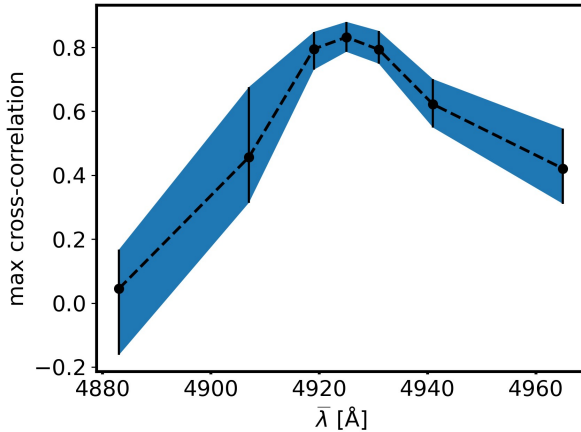


Fig. 1. NGC 4748: Maximum value of the cross correlation between the blue and the red part of the broad H β line, as a function of the dividing wavelength $\bar{\lambda}$. The peak of the cross-correlation is obtained when the line is divided in two equal-flux parts, i.e. when the signal-to noise-ratio is the highest for both the red and blue sides.

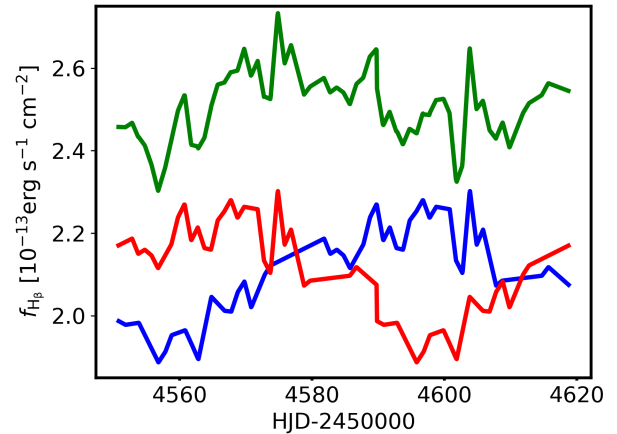


Fig. 2. NGC 4748: Original light-curve of the entire H β line (blue line), same light-curve shifted by half of the observational period (with periodic boundary conditions, red line), and the sum of the two (rigidly shifted toward lower fluxes for visualization purposes, green line), mimicking a MBHB whose components evolve independently on short timescales.

4. Application of FUVT to mock MBHBs

We apply FUVT to mock equal mass MBHBs generated by duplicating the temporal series of spectra of each of the nine single MBHs discussed above. One of the copies is shifted in time by half of the observational period (assuming periodic boundary conditions, as done in standard reverberation mapping studies). Since the magnitude of the time-shift τ_{shift} in the test is constrained to be smaller than 10 days, such a shift makes the evolution of the two series of spectra independent. The original and shifted light-curves (blue and red lines) of the whole H β for NGC 4748, together with the sum of the two (green line), mimicking the lightcurve of a MBHB, are shown in figure 2.⁷

The two series of spectra are then shifted in frequency, by the same amount, toward higher and lower wavelengths, respectively. The wavelength shifts are chosen in order to mimic circular MBHBs with periods of $\tau_{\text{orb}} = 50, 100, 300$ and 1000 yr, observed close to edge-on at the orbital phase that would maximize the Doppler effect. We chose such a configuration to check if, in the most favorable scenario, the test succeeds in identify binaries. Different configurations would result in smaller shifts between the two independent components of the BEL, and could in principle result in a missed detection. Notice that, while all the four periods fulfill the criterion set in equation 4, $\tau_{\text{orb}} = 50, 100$ would correspond to separations at which a sizable part of a disc-like BLR would be unstable. Furthermore, for those periods the outer parts of the BLR would be removed, resulting in a more “boxy” profile of each BEL component (see, e.g. [Nguyen et al. 2019](#)), while only a few of the AGN discussed in section 3 have a boxy broad H β . For these reasons from here on we will consider binaries with $\tau_{\text{orb}} = 300$ and 1000 yr as “solid” binaries, while keeping the $\tau_{\text{orb}} = 50$ and 100 yr binaries to highlight how the performances of our test scale with the orbital period and to account for possible alternative geometries and dynamics of the BLR.

⁷ We acknowledge that we could also enforce not-causally related lightcurves by using two different AGN. Unfortunately, due to the limited number of single MBHs, only 2 pairs have a small enough redshift difference to be interpreted as a relative velocity between two loosely bound MBHs. We defer the investigation of “heterogeneous” mock binaries to a future investigation.

We then add the two series up (adding the original errors in quadrature for each wavelength bin), obtaining four new mock MBHBs for each original MBH, for a grand total of 36 mock MBHBs. The upper panel of figure 3 shows an example of mock MBHB spectrum based on the observations of NGC 4748, without the application of any time shift for clarity purposes, and for a binary with $\tau_{\text{orb}} = 50$ yr. In the lower panel the resulting line profile starting from the same spectrum are shown for four different mock binary periods.

We then apply FUVT to these new sets of mock spectra. The resulting profile of $\max - CCF(\bar{\lambda})$ as a function of $\bar{\lambda}$ for the four mock MBHBs constructed starting from NGC 4748 are shown in figure 4.

The four mock binaries show clearly different $\max - CCF(\bar{\lambda})$ profiles with respect to the single MBH case. They tend to have values of $\max - CCF(\bar{\lambda})$ significantly smaller than the single MBH cases close to the bulk of the broad line: the shorter the period, the larger the frequency separation between the binary components contributions, the lower the $\max - CCF(\bar{\lambda})$. The highest values of the mock MBHB cross-correlation are instead found close to the line wings, where a correlation might be found due to the low signal to noise ratio of one of the two sides of the line. The anti-correlation observable for central values of $\bar{\lambda}$ is due to the shape of the broad H β light-curve, featuring a single peak appearing after a dimmer state (see figure 2 and the following discussion in this section). Such an anti-correlation should not be considered a solid feature associated to binaries, and, indeed, it is not observed in some of the other systems. Notice that even the mock binary with a 1000 yr period shows a clear minimum in the $\max - CCF(\bar{\lambda})$ profile, with the two parts of the line being almost completely uncorrelated, regardless the relatively small velocity shift between the two components associated to the two MBHs. In this case the relative velocity between the two MBHs is ≈ 500 km/s (equivalently, the shift of one of the peaks w.r.t. the centroid is ≈ 250 km/s), and the FWHM of the H β line is ≈ 2000 km/s ($\sigma \approx 1000$ km/s) in the mean spectrum for NGC4748. If we consider the varying component only looking at the RMS spectrum for the same system we get $\text{FWHM} \approx 1200$

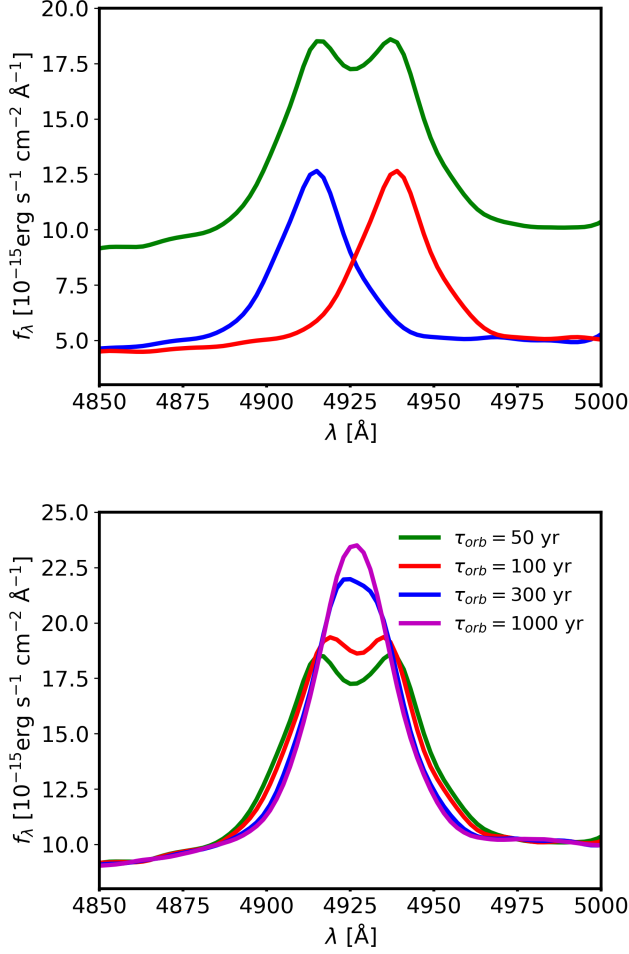


Fig. 3. NGC 4748. Upper panel: broad H β component of a mock spectrum shifted red-wards (red line) and blue-wards (blue line) to mimic the orbital velocity of an equal-mass MBHB with orbital period $\tau_{\text{orb}} = 50$ yr. The green line shows the composite line associated to the mock MBHB. Lower panel: composite broad H β lines for mock MBHBs with $\tau_{\text{orb}} = 50, 100, 300$ and 1000 yr (green, red, blue and magenta lines, respectively). The Doppler shifts are evaluated assuming an edge-on circular binary with the MBH velocities perfectly aligned with the line of sight.

km/s ($\sigma \approx 650$ km/s)⁸. While the velocity shift is smaller than the FWHM, our test still manages to identify the mock as a binary.

More generally, four other sets of mock binaries based on other observed AGN show trends that are qualitatively similar to the one shown in figure 4, three sets have values of \overline{CCF} that can be higher or lower than that of the single MBH case depending on the choice of orbital period, and one set has lower \overline{CCF} compared to the corresponding single MBH that, however, remain quite high, up to ≈ 0.75 . One example of mock binaries for each of the last two classes is shown in figure 5⁹. The occurrence of different behaviors is not surprising, since the actual profile of $\max - CCF(\bar{\lambda})$ depends mostly on the shape of the original

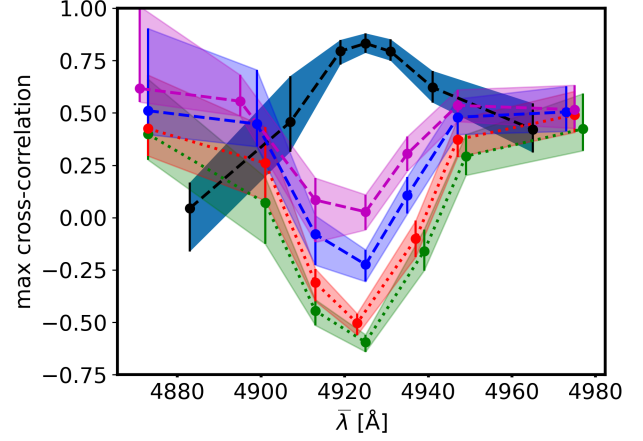


Fig. 4. Same as figure 1 for the four mock MBHBs obtained from NGC 4748. The green, red, cyan and magenta points with uncertainties are for binaries with $\tau_{\text{orb}} = 50, 100, 300$ and 1000 yr, respectively. The original values and uncertainties of NGC 4748 are shown in blue for comparison. “Solid” binaries are shown with dashed lines, while for shorter period binaries dotted lines are used.

H β light-curve used to generate the mock binary. If the original H β light-curve displays a single peak and single drop with similar duration, the corresponding binaries will tend towards anti-correlation when two-close-to-equal-flux parts of the composite H β are considered. If the original H β light-curve shows instead a more rapid variability the shift of half of the duration of the observations may result in close to zero correlation. If instead, e.g., the H β light-curve shows two peaks and two troughs with similar duration and equally-spaced, the time shift will not reduce significantly the maximum cross-correlation. We stress that such a variety of behaviours is due to the limited time-extent of the spectroscopic monitoring campaigns. In principle, in the binary scenario, an arbitrarily long campaign would have a collection of BEL profiles (one per pointing) that are contributed from the two completely uncorrelated components (1 and 2) associated to the two MBHBs. In this case, when cross-correlating the blue and the red part of the total BEL, the cross terms in the cross-correlation would be equal to zero¹⁰. The cross correlation between the two sides of the BEL would then read:

$$\begin{aligned} CCF(r, b, \tau) &= CCF(r_1 + r_2, b_1 + b_2, \tau) \\ &= \frac{\sigma(r_1)\sigma(b_1)}{\sigma(r_1+r_2)\sigma(b_1+b_2)} CCF(r_1, b_1, \tau) \\ &\quad + \frac{\sigma(r_2)\sigma(b_2)}{\sigma(r_1+r_2)\sigma(b_1+b_2)} CCF(r_2, b_2, \tau), \end{aligned} \quad (5)$$

where $\sigma(x)$ is the standard deviation of the x quantity. In the simplifying case in which the time delay maximizing the cross-correlation is the same for the two components, as for the case of our mock binaries, we obtain:

$$\begin{aligned} CCF(r, b, \tau_{\text{max}}) &= \frac{\sigma(r_1)\sigma(b_1)}{\sigma(r_1+r_2)\sigma(b_1+b_2)} CCF(r_1, b_1, \tau_{\text{max}}) \\ &\quad + \frac{\sigma(r_2)\sigma(b_2)}{\sigma(r_1+r_2)\sigma(b_1+b_2)} CCF(r_2, b_2, \tau_{\text{max}}). \end{aligned} \quad (6)$$

From eqs. 5 and 6 we can derive some interesting trends and limits: when the shifts of the two components (due to the velocity

¹⁰ I.e. the red part of component 1 (r_1) would have a zero cross-correlation with the blue part of component 2 (b_2).

⁸ All the values of σ and FWHM obtained from our analysis are consistent with those presented in (Bentz et al. 2009b).

⁹ The profiles of $\max - CCF(\bar{\lambda})$ for all the other single MBHBs and mock binaries are available at <https://astro.fisica.unimib.it/spectroscopical-search-of-massive-black-hole-binaries/>.

of the two MBHs along the line of side) tends to 0, and the line is split roughly in half, the denominator of the σ -ratios tends to $2\sigma(r_1)\sigma(b_1) \approx 2\sigma(r_2)\sigma(b_2)$, and the cross-correlation in eq. 5 and 6 tends to the arithmetic average of the cross-correlation between the blue and red parts of the two single components. If these cross-correlations are high (as expected for the a single MBH-BLR system, see section 3), the total cross-correlation will be equally high, as expected for a zero velocity-shift of the two components. On the other hand, the maximum cross-correlation in eq. 6 will become lower and lower (while remaining positive) the more the two components 1 and 2 are shifted from the reference frame of the galaxy and contribute more asymmetrically to the red and blue part of the whole line. Unfortunately, in many cases (as those considered in this paper) the length of the RM campaigns will not be sufficient to ensure that the two components are completely uncorrelated, leading to the variety of outcomes commented above. The dependence of the profile of $\max - CCF(\bar{\lambda})$ for binaries on the specific realization of the variability observed during the RM campaign has important implications for the identification of the studied systems as MBHBs. In next section we further discuss this point.

In principle, with a sufficiently large population of single MBHs studied with RM constraining the distribution of \overline{CCF} in the line bulk (i.e. measured for one of the three central $\bar{\lambda}$), we could translate the values of \overline{CCF} of our mock binaries into a probability of not belonging to the “standard” population. To date such distribution is largely unconstrained. As an example, in figure 6 we show the distributions of \overline{CCF} for the observed single MBHs discussed in section 3 (blue histogram) and the mock binaries (red histograms). The two distributions are clearly different. Starting from the observed \overline{CCF} for the nine AGNs, we construct a model of the \overline{CCF} distribution for “typical” single MBH that we then use to infer the probability of mocks to belong to the single MBH population. Our model is based on the assumption that (i) the population of single MBHs has a well defined value of \overline{CCF} , and that (ii) the red and blue parts of the H β flux data follow a bi-variate Gaussian distribution, with the aforementioned, unknown, correlation coefficient \overline{CCF} . The latter allows to exploit the analytical form for the sampling distribution of the \overline{CCF} derived by Fisher (1928), given a set of observed \overline{CCF}_i . We infer a posterior distribution for \overline{CCF} using a nested sampling algorithm, that we use as the model for the expected distribution of measured \overline{CCF} for single MBHs. The cumulative probability of observing a given value of \overline{CCF} (again restricting our search to the bulk of the BELs) is shown as the black curve in figure 6. The vertical blue and red ticks highlight the values of \overline{CCF} measured for all the observed single and mock binaries in the bulk of the BEL. Mocks with lower values of \overline{CCF} have lower probabilities, with 24 (out of 36) mocks having a probability $< 10^{-3}$. The values of \overline{CCF} and of the associated probabilities are reported in table 1.¹¹

5. Discussion

We presented a novel method (FUVT) to search for MBHBs and to test the binary hypothesis in already identified MBHB candidates. The method is tailored to seek large separation binaries,

when the two MBHs can retain their own BLR, with orbital periods that can be $\gtrsim 50$ yr. FUVT assumes that the two MBHs are at sufficiently large distances to ensure that the short term variability of the two BLRs are uncorrelated. A simple correlation test between the long- and short-wavelength parts of BELs can therefore identify binaries if the maximum cross-correlation (once the BELs are split in two comparable flux components) is small enough compared to the high level of correlation expected and observed for single MBHs.

Differently from the already proposed SPT, that requires follow-up campaigns at least as long as $\sim \tau_{\text{orb}}$ to track the expected evolution of the orbital velocity of one active component of the binary, FUVT works on significantly shorter observational campaigns. The expected timescales of the test are from weeks to few years in the worse case scenario, provided that a sufficiently frequent time coverage (typical of reverberation mapping studies) of the candidate spectra is achieved.

In addition to the obvious advantage of its short duration, FUVT has a number of specific advantages and disadvantages with respect to SPT, making the two procedures complementary:

- FUVT performs best when the two MBHs in the binary have, on average, similar BEL luminosities. According to theoretical studies (e.g. Roedig et al. 2012; Duffell et al. 2020, and references therein) secondary MBHs are expected to experience higher accretion rates, making FUVT particularly relevant either for close to equal mass (and equal Eddington ratio) systems or for systems in which the secondary luminosity is close to its Eddington limit. If the flux coming from one of the two BLRs is too small compared to the other, FUVT could fail in distinguishing the subdominant contribution from the observational noise;
- if however the two MBHs contribute similarly to the BELs, the previously proposed tests (and SPT in particular) could miss real binaries, since, at large separations, no double peaked profile could be detectable (see, e.g. fig 3) or could be misinterpreted as the indication of a disc-like BLR, as in the standard interpretation for the broad double-peaked emitters (e.g. Eracleous & Halpern 1994). Even if a binary is selected as a candidate at a time when one MBH was significantly brighter than the other, SPT could fail in observing a long term frequency shift consistent with the orbital evolution of a binary, if the other component undergoes a sizable re-brightening changing the shape (and centroid) of the line. Such an evolution could result in the erroneous dismissal of real binaries if SPT only is performed, while the binary nature of the system would be easily identifiable by FUVT;
- as discussed in section 4, the stochastic nature of the short term variability of each MBH accretion disc can occasionally result in high cross-correlations even if the observed AGN hosts a real MBHB. If FUVT is applied to large spectroscopic catalogues to identify new MBHB candidates, a fraction of the MBHBs in the data are expected not to be identified. It is difficult to estimate a solid missed detection fraction, due to the small number of single MBHs that we use to characterize the “control sample”. However, taking the probabilities we estimated (with a priori assumptions on the shape of $p(\text{CC})$, to be verified when enough data will be available), and assuming as “missed” alarm threshold of $p \geq 0.01$ (corresponding to $\text{CC} \geq 0.70$), we get 10 systems out of 36 ($\approx 28\%$ of missed binaries) including binaries with a period shorter than 300 yr, or 9 out of 18 when considering only larger “solid” binaries (see the discussion in section 2). Such shortcoming can be circumvented when

¹¹ We stress that the somewhat low probability values for two of the single MBHs (Mrk142 and NGC5548) should be considered with caution, since the functional form of the probability distribution has been decided a priori for this exercise.

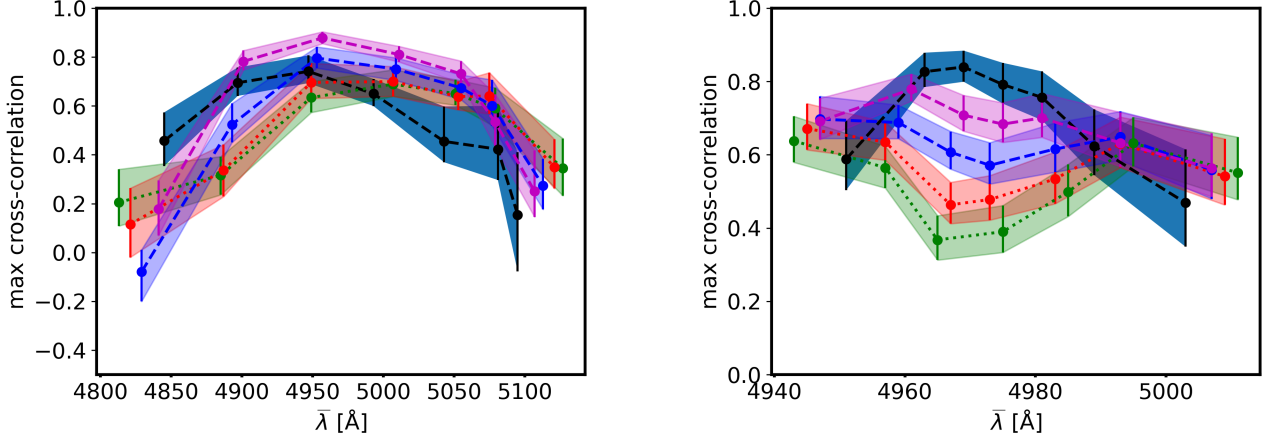


Fig. 5. Same as figure 4 for NGC 5548 and the associated mock binaries (left panel) and for Mrk 202 (right panel). The case on the left represents a class of objects in which the max cross-correlation in the bulk of the broad line can be higher or lower than that of the single MBH depending on the assumed period. The right panel shows the only case in which the single MBH has a value of \overline{CCF} higher than any of its sibling mock binaries, but the cross-correlation of the mocks can be quite high, up to ~ 0.75 for the shortest period. Please note that the y axis change from panel to panel to emphasize the differences between the different cases.

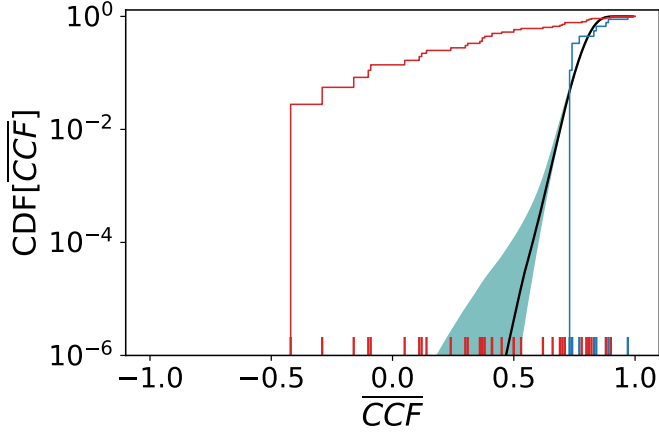


Fig. 6. Blue (red) histogram: normalized cumulative distribution of the observed single (mock binaries) MBHs. The solid black line shows the median cumulative probability of a system to have \overline{CCF} lower than a given value (obtained from the single MBH data under the assumptions specified in the text). The teal band indicates the 90% credible region for the cumulative distribution of \overline{CCF} for single MBHs. The vertical red (blue) ticks highlight the \overline{CCF} values for all the 36 mock binaries (9 single MBHs). The numerical values of all the \overline{CCF} and cumulative probabilities listed in table 1

FUVT is applied to data taken from still frequent but significantly longer campaign, motivated, for example, by an independent identification of a source as a promising MBHB candidates. In this case, if the first observational campaign finds a high correlation in the red and blue part of BELs, the test should be considered inconclusive, and a new campaign should be performed. Only after a few campaigns (for a total of a few years, in the worse case scenario), the binary hypothesis can be ruled out (unless a low correlation period is found, in which case the binary nature is indeed confirmed). Note however that the missed detection fraction estimated here cannot be used to infer the statistics of the global MBHB population, since, in this first method paper, we are consid-

ering only the idealized edge-on/Doppler-maximising configuration for equal mass binaries. A broader analysis of the binary parameter space, including the statistical estimate of the minimum number of observational campaigns needed to disprove the MBHB scenario with a given confidence, are postponed to a future study;

- finally, we stress that all the currently spectroscopically selected MBHB candidates have masses $\gtrsim 10^8 M_\odot$ (e.g. Tsalmantza et al. 2011; Eracleous et al. 2012), and no candidates in the $10^5 - 10^7 M_\odot$ range of interest for the future gravitational wave interferometer LISA have been identified yet. This might be due to a selection effect specific of the traditional spectroscopic search. Indeed, in order to be selected as MBHB candidates, the BELs are typically required to be shifted by $\gtrsim 1000 \text{ km s}^{-1}$ (Tsalmantza et al. 2011; Eracleous et al. 2012) with respect to the host rest frame (traced by the narrow emission lines), to prevent the inclusion of single MBHs with slightly asymmetric BLRs. Such threshold can be higher than the maximum velocity for which the secondary of a MBHB can retain its own BLR¹²:

$$v_2 \approx 480 \text{ km s}^{-1} \times \left(\frac{M_2}{10^6 M_\odot} \right)^{0.24} f_{\text{Edd}}^{-0.26} f(q)^{-0.5}, \quad (7)$$

where

$$f(q) = q^{1/3} (1 + q) \left[0.6q^{2/3} + \ln(1 + q^{1/3}) \right], \quad (8)$$

for small secondary masses and close to equal mass binaries, unless the Eddington ratio is small. E.g., $M_2 = 10^6 M_\odot$ and $q = 1$ would require a $f_{\text{Edd}} \lesssim 0.01$ to have a maximum secondary velocity of $v_2 \approx 1000 \text{ km s}^{-1}$. For such small masses and low f_{Edd} collecting a spectrum with enough signal-to-noise to perform the test might be prohibitively challenging. FUVT, however, could still succeed in identifying a MBHB (as it does for three mock MBHBs with periods of 1000 yr), if the random fluctuations of the two MBHs do not appear correlate by chance (see the discussion above).

¹² As eq. 4, obtained equating eq. 2 and eq. 3. For “solid” binaries the criterion would be even more constraining.

As a final note, we stress that the procedure we discussed could, in principle, identify false MBHB positives if the structure of the BLR around a single MBH is sufficiently complex, with strong asymmetries including, e.g., long-lived spiral waves (e.g. [Storchi-Bergmann et al. 2003](#)) or hot spots (e.g. [Fries et al. 2023](#)). If a large and representative distribution of \overline{CCF} would be available for bona-fide symmetric single MBHs, FUVT could identify sub-populations of outliers. Their deviation from a reference \overline{CCF} distribution would give an estimate of the probability that such systems do not belong to the “normal” single MBH distribution (as exemplified in section 4), allowing for the selection of candidates to be further analysed to discriminate between the two (asymmetric single BLR and MBHB) scenarios. We speculate that the inclusion of the information on the cross-correlation of the two (blue and red) parts of the BELs with the observed continuum could inform about the most plausible scenario. A study quantifying false positives, i.e. AGN with single asymmetric BELs, and developing tests to identify them is ongoing. Still, we believe that currently the most limiting factor is the paucity of systems for which reverberation mapping studies have been performed. Indeed, in order to estimate the probability that our mock MBHBs are outliers of the single MBH distribution, in section 4 we had to assume an *a priori* \overline{CCF} distribution for single MBHs, as nine measurements were barely enough to characterize such distribution. The situation will, however, improve significantly thanks to future large reverberation mapping campaigns (e.g. the black hole mapper program of the SDSS-V, [Almeida et al. 2023](#)), adding ~ 1000 systems to the current sample, thus allowing a far better determination of the single MBHs distribution of \overline{CCF} . With a large enough sample, one could even begin to identify subpopulations within the single MBH class, ultimately leading to a more accurate identification of binary MBHs candidates. An alternative improvement could be achieved with a dedicated reverberation mapping campaign on double peaked emitters¹³. Such study could provide an additional test on the nature of individual double peaked emitters (see also [Eracleous et al. 1997](#); [Liu et al. 2016](#), for different tests) and, even if all the systems will prove to be single MBHs with disk like BELs (e.g. [Eracleous & Halpern 1994](#)), could serve as comparison for future candidates.

Acknowledgements. The Authors thank G. De Rosa and M. Bentz for their help with the RM datasets, and M. Eracleous, Z. Haiman and D.J.D’Orazio for their useful comments and suggestions. MD acknowledge funding from MIUR under the grant PRIN 2017-MB8AEZ, and financial support from ICSC – Centro Nazionale di Ricerca in High Performance Computing, Big Data and Quantum Computing, funded by European Union – NextGenerationEU. RB acknowledges support through the Italian Space Agency grant *Phase A activity for LISA mission, Agreement n. 2017-29-H.0, CUP F62F17000290005*.

References

Ackermann, M., Ajello, M., Albert, A., et al. 2015, *ApJ*, 813, L41
 Almeida, A., Anderson, S. F., Argudo-Fernández, M., et al. 2023, *ApJS*, 267, 44
 Amaro-Seoane, P., Andrews, J., Arca Sedda, M., et al. 2023, *Living Reviews in Relativity*, 26, 2
 Amaro-Seoane, P., Audley, H., Babak, S., et al. 2017, *arXiv e-prints*, arXiv:1702.00786
 Begelman, M. C., Blandford, R. D., & Rees, M. J. 1980, *Nature*, 287, 307
 Bentz, M. C., Peterson, B. M., Netzer, H., Pogge, R. W., & Vestergaard, M. 2009a, *ApJ*, 697, 160
 Bentz, M. C., Walsh, J. L., Barth, A. J., et al. 2009b, *ApJ*, 705, 199
 Blandford, R. D. & McKee, C. F. 1982, *ApJ*, 255, 419

Bortolas, E., Bonetti, M., Dotti, M., et al. 2022, *MNRAS*, 512, 3365
 Bortolas, E., Capelo, P. R., Zana, T., et al. 2020, *MNRAS*, 498, 3601
 Burke-Spolaor, S. 2011, *MNRAS*, 410, 2113
 Charisi, M., Bartos, I., Haiman, Z., et al. 2016, *MNRAS*, 463, 2145
 Chen, Y.-C., Liu, X., Liao, W.-T., et al. 2020, *MNRAS*, 499, 2245
 Davelaar, J. & Haiman, Z. 2022a, *Phys. Rev. D*, 105, 103010
 Davelaar, J. & Haiman, Z. 2022b, *Phys. Rev. Lett.*, 128, 191101
 Decarli, R., Dotti, M., Fumagalli, M., et al. 2013, *MNRAS*, 433, 1492
 del Valle, L., Escala, A., Maureira-Fredes, C., et al. 2015, *ApJ*, 811, 59
 D’Orazio, D. J. & Di Stefano, R. 2018, *MNRAS*, 474, 2975
 D’Orazio, D. J., Haiman, Z., & Schiminovich, D. 2015, *Nature*, 525, 351
 Dotti, M., Bonetti, M., D’Orazio, D. J., Haiman, Z., & Ho, L. C. 2022, *MNRAS*, 509, 212
 Dotti, M., Bonetti, M., Rigamonti, F., et al. 2023, *MNRAS*, 518, 4172
 Duffell, P. C., D’Orazio, D., Derdzinski, A., et al. 2020, *ApJ*, 901, 25
 Eggleton, P. P. 1983, *ApJ*, 268, 368
 Eracleous, M., Boroson, T. A., Halpern, J. P., & Liu, J. 2012, *ApJS*, 201, 23
 Eracleous, M. & Halpern, J. P. 1994, *ApJS*, 90, 1
 Eracleous, M., Halpern, J. P., M. Gilbert, A., Newman, J. A., & Filippenko, A. V. 1997, *ApJ*, 490, 216
 Fiacconi, D., Mayer, L., Roškar, R., & Colpi, M. 2013, *ApJ*, 777, L14
 Fisher, R. A. 1928, *Proceedings of the Royal Society of London. Series A, Containing Papers of a Mathematical and Physical Character*, 121, 654
 Fries, L. B., Trump, J. R., Davis, M. C., et al. 2023, *ApJ*, 948, 5
 Gaskell, C. M. 1996, in *Jets from Stars and Galactic Nuclei*, ed. W. Kundt, Vol. 471, 165
 Graham, M. J., Djorgovski, S. G., Stern, D., et al. 2015, *MNRAS*, 453, 1562
 Hayasaki, K., Mineshige, S., & Ho, L. C. 2008, *ApJ*, 682, 1134
 Ju, W., Greene, J. E., Rafikov, R. R., Bickerton, S. J., & Badenes, C. 2013, *ApJ*, 777, 44
 Kaspi, S., Smith, P. S., Netzer, H., et al. 2000, *ApJ*, 533, 631
 Li, Y.-R., Wang, J.-M., Ho, L. C., et al. 2016, *ApJ*, 822, 4
 Li, Y.-R., Wang, J.-M., Zhang, Z.-X., et al. 2019, *ApJS*, 241, 33
 Liu, J., Eracleous, M., & Halpern, J. P. 2016, *ApJ*, 817, 42
 Liu, T., Gezari, S., Ayers, M., et al. 2019, *ApJ*, 884, 36
 Montuori, C., Dotti, M., Colpi, M., Decarli, R., & Haardt, F. 2011, *MNRAS*, 412, 26
 Nguyen, K., Bogdanović, T., Runnoe, J. C., et al. 2019, *ApJ*, 870, 16
 Peterson, B. M., Ferrarese, L., Gilbert, K. M., et al. 2004, *ApJ*, 613, 682
 Peterson, B. M., Wanders, I., Horne, K., et al. 1998, *PASP*, 110, 660
 Rodriguez, C., Taylor, G. B., Zavala, R. T., Pihlström, Y. M., & Peck, A. B. 2009, *ApJ*, 697, 37
 Roedig, C., Sesana, A., Dotti, M., et al. 2012, *A&A*, 545, A127
 Runnoe, J. C., Eracleous, M., Mathes, G., et al. 2015, *ApJS*, 221, 7
 Runnoe, J. C., Eracleous, M., Pennell, A., et al. 2017, *MNRAS*, 468, 1683
 Sandrinelli, A., Covino, S., Dotti, M., & Treves, A. 2016, *AJ*, 151, 54
 Sandrinelli, A., Covino, S., Treves, A., et al. 2018, *A&A*, 615, A118
 Severgnini, P., Ciccone, C., Della Ceca, R., et al. 2018, *MNRAS*, 479, 3804
 Shen, Y., Liu, X., Loeb, A., & Tremaine, S. 2013, *ApJ*, 775, 49
 Shen, Y. & Loeb, A. 2010, *ApJ*, 725, 249
 Songsheng, Y.-Y., Xiao, M., Wang, J.-M., & Ho, L. C. 2020, *ApJS*, 247, 3
 Souza Lima, R., Mayer, L., Capelo, P. R., & Bellovary, J. M. 2017, *ApJ*, 838, 13
 Storchi-Bergmann, T., Nemmen da Silva, R., Eracleous, M., et al. 2003, *ApJ*, 598, 956
 Storchi-Bergmann, T., Schimoia, J. S., Peterson, B. M., et al. 2017, *ApJ*, 835, 236
 Sun, M., Grier, C. J., & Peterson, B. M. 2018, *PyCCF: Python Cross Correlation Function for reverberation mapping studies*, *Astrophysics Source Code Library*, record ascl:1805.032
 Tamburello, V., Capelo, P. R., Mayer, L., Bellovary, J. M., & Wadsley, J. W. 2017, *MNRAS*, 464, 2952
 Tsalmantza, P., Decarli, R., Dotti, M., & Hogg, D. W. 2011, *ApJ*, 738, 20
 Valtonen, M. J., Lehto, H. J., Nilsson, K., et al. 2008, *Nature*, 452, 851
 Verbiest, J. P. W., Lentati, L., Hobbs, G., et al. 2016, *MNRAS*, 458, 1267
 Wang, J.-M., Songsheng, Y.-Y., Li, Y.-R., & Yu, Z. 2018, *ApJ*, 862, 171
 Wang, L., Greene, J. E., Ju, W., et al. 2017, *ApJ*, 834, 129

¹³ The two approaches do not necessarily need independent observational campaigns, as double peaked components might be frequent (or even ubiquitous) in type I AGN ([Storchi-Bergmann et al. 2017](#)).

Table 1. Values of \overline{CCF} and the associated probability of belonging to the distribution of single MBHs for single and (mock) binary MBH

name	\overline{CCF}	P	“solidity”
Mrk142	0.73	0.04	
SBS1116+583A	0.77	0.2	
Arp151	0.97	> 0.99	
Mrk1310	0.89	> 0.99	
Mrk202	0.84	0.71	
NGC4253	0.74	0.06	
NGC4748	0.83	0.64	
NGC5548	0.74	0.06	
NGC6814	0.88	0.97	
Mrk142_50	0.66	< 10 ⁻³	
Mrk142_100	0.71	0.01	
Mrk142_300	0.78	0.26	solid
Mrk142_1000	0.81	0.49	solid
SBS1116+583A_50	0.38	< 10 ⁻³	
SBS1116+583A_100	0.37	< 10 ⁻³	
SBS1116+583A_300	0.41	< 10 ⁻³	solid
SBS1116+583A_1000	0.45	< 10 ⁻³	solid
Arp151_50	-0.42	< 10 ⁻³	
Arp151_100	-0.29	< 10 ⁻³	
Arp151_300	-0.09	< 10 ⁻³	solid
Arp151_1000	0.14	< 10 ⁻³	solid
Mrk1310_50	0.05	< 10 ⁻³	
Mrk1310_100	0.12	< 10 ⁻³	
Mrk1310_300	0.24	< 10 ⁻³	solid
Mrk1310_1000	0.41	< 10 ⁻³	solid
Mrk202_50	0.5	< 10 ⁻³	
Mrk202_100	0.53	< 10 ⁻³	
Mrk202_300	0.62	< 10 ⁻³	solid
Mrk202_1000	0.71	0.01	solid
NGC4253_50	0.3	< 10 ⁻³	
NGC4253_100	0.37	< 10 ⁻³	
NGC4253_300	0.36	< 10 ⁻³	solid
NGC4253_1000	0.5	< 10 ⁻³	solid
NGC4748_50	-0.16	< 10 ⁻³	
NGC4748_100	-0.1	< 10 ⁻³	
NGC4748_300	0.11	< 10 ⁻³	solid
NGC4748_1000	0.31	< 10 ⁻³	solid
NGC5548_50	0.69	0.004	
NGC5548_100	0.7	0.008	
NGC5548_300	0.8	0.4	solid
NGC5548_1000	0.88	0.97	solid
NGC6814_50	0.8	0.41	
NGC6814_100	0.82	0.56	
NGC6814_300	0.9	> 0.99	solid
NGC6814_1000	0.9	> 0.99	solid

Notes. The values of \overline{CCF} are restricted to the bulk of the line, while the associated probability of belonging to the distribution of single MBHs have been calculated using the median cumulative distribution for \overline{CCF} , solid line in Fig. 6. The name of the mocks are constructed by attaching the period of the binary (in yr) to the name of the real AGN progenitor. The last column identifies the “solid” binaries, for which a stable disc-like BLR can exist around both MBHs. Considering that our inferred cumulative distribution for the \overline{CCF} is well determined up to probabilities as low as $\sim 10^3$, we consider smaller values as upper limits.